16th World Conference on Earthquake, 16WCEE 2017
Santiago Chile, January 9th to 13th 2017
Paper N° 4437
Registration Code: S-S1461406315

VERIFICATION OF SUBSURFACE S-WAVE VELOCITY STRUCTURE MODEL IN IWAKI CITY, FUKUSHIMA PREFECTURE, USING A DENSE SEISMIC ARRAY

T. Hayashida[(1)], H. Nakagawa[(2)], T. Yokoi[(3)], S. Koyama[(4)], T. Kashima[(5)], and S. Nagano[(6)]

[(1)] *Senior Research Scientist, International Institute of Seismology and Earthquake Engineering, Building Research Institute, Japan, takumi-h@kenken.go.jp*
[(2)] *Senior Research Engineer, Department of Structural Engineering, Building Research Institute, Japan, hiroto-n@kenken.go.jp*
[(3)] *Director, International Institute of Seismology and Earthquake Engineering, Building Research Institute, Japan, tyokoi@kenken.go.jp*
[(4)] *Research Coordinator for Quality Control of Building, Building Department, National Institute for Land and Infrastructure Management, Japan, koyama-s92hs@nilim.go.jp*
[(5)] *Senior Research Engineer, International Institute of Seismology and Earthquake Engineering, Building Research Institute, Japan, kashima@kenken.go.jp*
[(6)] *Assistant Manager, OYO Corporation, Japan, nagano-shuichi@oyonet.oyo.co.jp*

Abstract

A dense seismic/microtremor array consisting of 16 sensors was deployed in Iwaki city, Fukushima prefecture, Japan from November 2014 to September 2015. During the observation period, seismic signals from at least 100 felt earthquakes ($3.5 \leq Mw \leq 7.9$) as well as continuous microtremors were recorded. In this study we used the event data to investigate site amplification factors beneath the observation sites and also used microtremor data to estimate propagation properties of surface wave in the entire area, for the verification of an existing three-dimensional seismic velocity structure model. The site amplification factors estimated from spectral inversion method indicate the spatial variations of subsurface soil structure and the Rayleigh-wave dispersion properties derived from the seismic interferometry technique show lower group velocities compared with the theoretical curve from the existing model. On the other hand, predicted dominant frequency and group velocity of Rayleigh wave based on one-dimensional S-wave structure model from large-scale microtremor array survey show similar trends with the estimations. The results show that the combined use of the dense microtremor and strong motion data in a local area of high seismicity can be a powerful tool for the improvement of subsurface structure model.

Keywords: Array observation, Spectral inversion, Seismic interferometry, Group velocity, Surface wave dispersion

1. Introduction

Iwaki city is located in the southeastern part of Fukushima prefecture, northeast Japan (Tohoku region), along the Pacific coast. The greater part of the city is geologically located in the southeastern of the Abukuma mountains (Abukuma belt) where old metamorphic rocks are widely exposed. On the other hand, in the east part of the city, the Miocene sedimentary rocks are distributed on hills and small-scale sedimentary basins including the central area (Taira and Uchigo districts) have been formed by the late Pleistocene and Holocene alluvial deposits. The city was affected by strong ground shakings during the 2011 off the Pacific coast of Tohoku Earthquake (Mw9.0), the 2011 Fukushima Hamadori earthquake (Mw6.6) and the successive aftershocks [1].

In Japan, fine-scale three-dimensional (3D) velocity structure models including subsurface soli layers ($Vs \geq 350$ m/s) have been constructed for ground motion hazard evaluation [2,3]. The models indicate that the seismic bedrock depth becomes gradually deeper toward the northeast in the central part of Iwaki city (see an example in Fig.1a). However, for cities that are remote from major cities in large seimentary basins (e.g. Tokyo, Yokohama, Osaka and Nagoya) like Iwaki city, the accuracy of the model is not well verified since the models were constructed by interpolating limited borehole data, geological information and gravity anomalies and there are not many seismic stations to compare synthetic seismograms with the data. Results of the previous

microtremor array surveys and surface wave explorations in the central area indicate the complicated subsurface soil structure that is not included in the published structure models [4,5].

In this study we use waveform data from a temporal seismic/microtremor observation array which was deployed in the central part of the city to investigate site amplification factors of the sedimentary basin and validate the accuracy of the current seismic velocity model, using both earthquake and microtremor recordings.

2. Observations of Microtremor and Strong Ground Motions

Offline observations of ground motions at 16 sites were performed in the central area of Iwaki city between November 2014 and September 2015. The array extends 8.5 km east to west by 5 km north to south, making it possible to investigate spatial variations of site amplification factors in the basin (Fig.1a). Here we deployed four different types of three-component sensors (Table 1) in order to observe earthquake ground motions as well as microtremors; two intermediate period seismometers (CMG-40T, Güralp Systems Ltd.), four over-damped accelerometers (SMAR-6A3P, Mitsutoyo Corporation), seven servo-type accelerometers (CV-374, Tokyo Sokushin Co., Ltd.) and three force-balanced accelerometers (Etna, Kinemetrics Inc.). Observations at stations TJ2, TJ3, TP3, TP4 and YSM were terminated at the end of July 2015 and the sensor at station MMY (Etna) was replaced by CMG-40T which had been used at station TP4 (see Table 1). At each station, the sampling frequency is 100 Hz and the observation system is located inside ground-floor room of low building in which building effect is small and electric power can be obtained by AC power supply. The north-south component of the sensors is fixed in the direction parallel to walls and the horizontal motions are converted into north-south and east-west directions later.

Except stations MMY, TJ2 and YSM where trigger type sensors were used, the continuous seismic data were recorded and earthquake ground motion data were manually extracted based on the information of recorded seismic intensity database provided by Japan Meteorological Agency (JMA). We selected earthquakes whose maximum intensity in Iwaki city is at least I on the JMA scale [6]. Finally, ground motion data from more than 100 felt earthquakes ($3.5 \leq Mw \leq 7.9$) were obtained. Most of the events are inter-plate and intra-plate earthquakes that occurred along off the Pacific coast (Figure 1b).

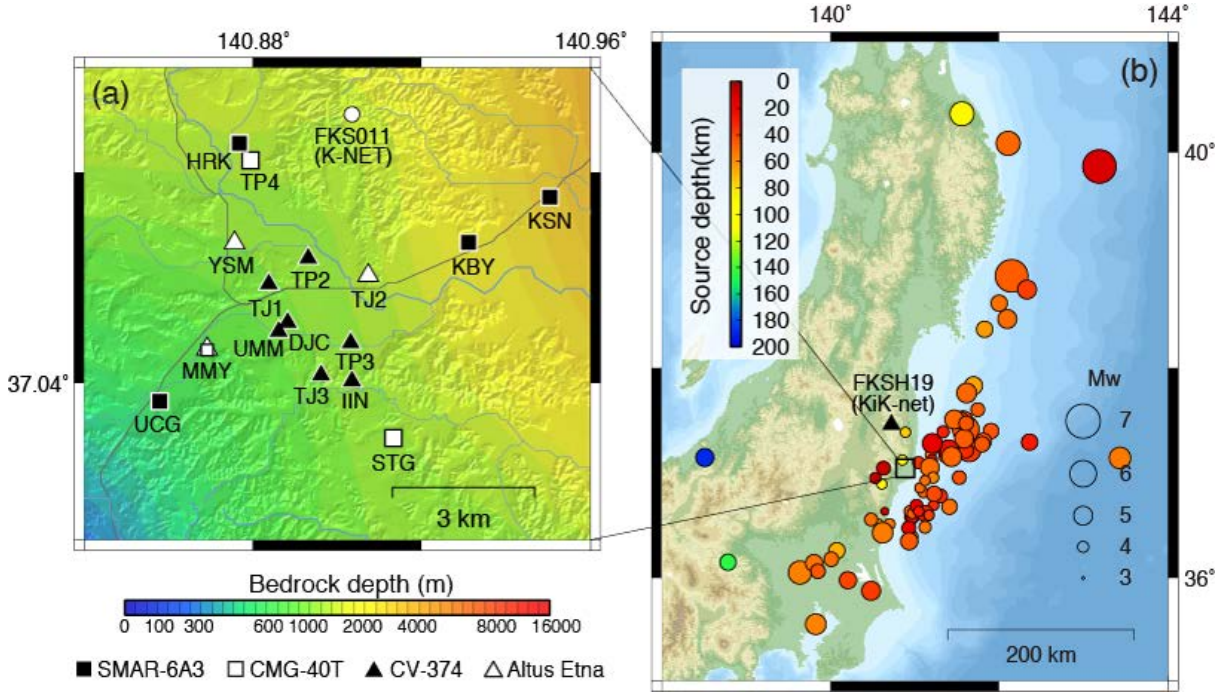

Fig. 1 – (a) Distribution of seismic stations and seismic bedrock depth (V_S=3.0km/s) in Iwaki city. (b) Distributions of observed 100 felt earthquakes during the observation period.

Table 1 – List of the stations used in this study.

Station code	Lat. (°)	Lon. (°)	Alt. (m)	Observation period (yy/mm/dd)	Sensor	Number of events
DJC	37.0515	140.8882	7	14/11/27 - 15/11/02	CV-374	65
HRK	37.0856	140.8768	14	14/11/28 - 15/09/29	SMAR-6A3P	75
IIN	37.0403	140.9035	21	14/11/28 - 15/09/28	CV-374	76
KBY	37.0667	140.9311	5	14/11/28 - 15/09/28	SMAR-6A3P	76
KSN	37.0753	140.9504	4	14/11/27 - 15/09/29	SMAR-6A3P	76
MMY[1]	37.0464	140.8691	9	14/11/28 - 15/06/23	Etna	22
MMY[2]	37.0464	140.8691	9	15/06/23 - 15/09/29	CMG-40T	-
STG	37.0295	140.9133	46	14/11/28 - 15/09/29	CMG-40T	73
TJ1	37.0588	140.8838	39	14/11/28 - 15/09/29	CV-374	52
TJ2	37.0604	140.9074	39	14/11/27 - 15/06/22	Etna	29
TJ3	37.0415	140.8962	14	14/11/27 - 15/06/22	CV-374	51
TP2	37.0637	140.8931	10	14/11/27 - 15/09/29	CV-374	52
TP3	37.0475	140.9032	8	14/11/27 - 15/05/13	CV-374	25
TP4	37.0823	140.8795	14	14/11/27 - 15/06/22	CMG-40T	47
UCG	37.0365	140.8579	12	14/11/27 - 15/09/20	SMAR-6A3P	74
UMM	37.0497	140.8862	7	14/11/27 - 15/09/10	CV-374	70
YSM	37.0666	140.8756	13	14/11/28 - 15/06/22	Etna	33
FKS011*	37.0911	140.9035	165	-	K-NET11A	55
FKSH19*	37.4703	140.7225	510	-	KiK-net06	61

* NIED stations

Figure 2 shows the stacked power spectral densities (PSDs) of the continuous seismic noise in the vertical component at stations KBY, STG and TJ1 during the period from January 1 to 31, 2015. Each PSD is computed using 327.68 s time window where there is no amplitude disturbances (e.g. strong artificial noises or earthquakes). The background seismic noise levels are significant between -130 and -100 dB in a broad period range at stations where the sensors SMAR-6A3P and CMG-40T were deployed. On the other hand, at stations where the sensor CV-374 is deployed, electrical noise is dominant above 0.15 s (≤ 6.7 Hz), indicating that the sensor cannot be used for microtremir analysis in this study.

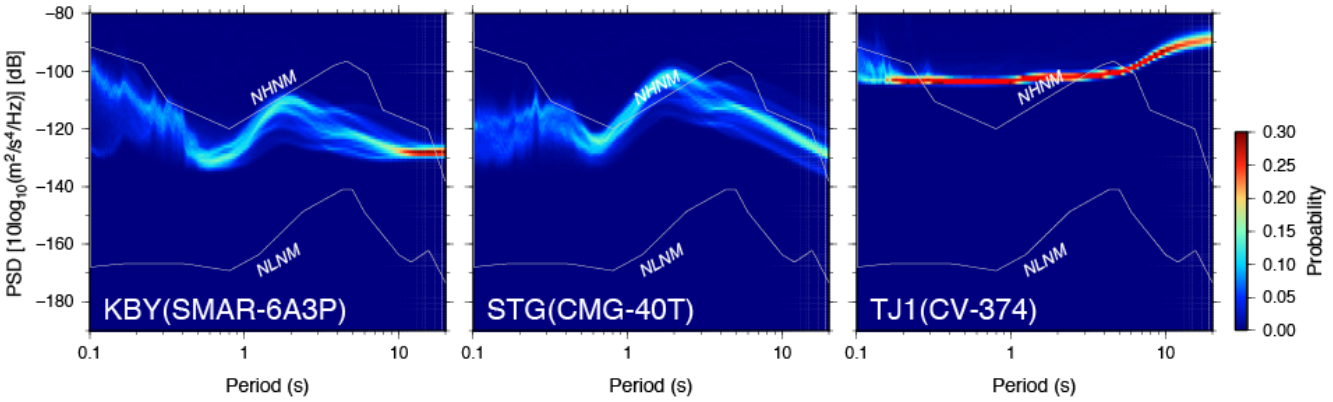

Fig. 2 – Examples of calculated power spectral densities (PSDs) using microtremor data.

3. Application of Spectral Inversion Technique to Event Data

3.1 Selection of event data

To estimate site amplification factors (i.e. seismic wave amplification characteristics between seismic bedrock and the ground surface) at 16 stations, spectral inversion technique is applied to the recorded event data. Our dataset includes waveforms from local crustal earthquakes to distant deep-focus earthquakes, but the mixture of various type earthquakes may cause significant errors in the results of the inversion since we assume depth-independent and directionally-independent (homogeneous) propagation path characteristics in our analysis. Then we selected recordings from 76 inter-plate or intra-plate earthquakes that occurred off the Pacific coast (30-400 km from the city center) and whose moment tensor solution is available in the catalogue of the National Research Institute for Earth Science and Disaster Resilience (NIED).

In the analysis, we also included acceleration data from the closest NIED K-NET [7] station to the array (FKS011; see the location in Fig.1a) to compare our result with the proposed amplification factor at the station. In addition, since the size of the obervation array is much smaller than hypocentral distances, we also add data recorded at NIED KiK-net station [8] FKSH19 (see the location in Fig.1b) where the site amplification factor is known to be nearly flat below 1 Hz [9]. At stations STG and TP4 where the velocity seismometers are deployed, the observed horizontal component waveforms were differentiated in the time domain to obtain accelerograms. We set the lower limit of the frequency range for the inversion to 0.3 Hz, since we confirmed that the shapes of the Fourier amplitude spectra coincide with each other above the frequency, regardless of sensor types.

3.2 Spectral inversion method

The observed Fourier spectra of *S*-wave portion in the frequency domain, $O_{ij}(f)$ for *i*-th earthquake observed at *j*-th station, is expressed as a linear combination of source, propagation path and site amplification factors [10],

$$O_{ij}(f) = S_i(f) G_j(f) R_{ij}^{-1} \exp\left[\frac{-\pi R_{ij} f}{Q_S(f)\beta}\right], \quad (1)$$

where $S_i(f)$ is the source term for *i*-th earthquake, $G_j(f)$ is the site amplification factor at *j*-th station. R_{ij}, β, and Q_S denote hypocentral distance between *i*-th earthquake and *j*-th site, averaged *S*-wave velocity and quality factor of *S*-wave in the propagation path, respectively. Here we assumed the value β = 3.6 km/s and there is no spatial variation in Q_S. The time windows of *S*-wave portion are extracted using the Husid plots [11], taking the interval between the times at which 5 and 95% of the cumulative squared acceleration. Here we excluded data whose maximum amplitude in the horizontal component is less than 0.5 gal. The *S*-wave spectra of NS and EW components were merged to obtain a horizontal component spectrum $O_{ij}(f)$ by computing the root-mean square average.

According to [12], the spectral ratios between *j*-th site and the divisor site *d* can be expressed as

$$\frac{O_{ij}(f)}{O_{id}(f)} = \frac{R_{id} G_j(f)}{R_{ij} G_d(f)} \exp\left[\frac{-\pi(R_{ij} - R_{id}) f}{Q_S(f)\beta}\right], \quad (2)$$

where the subscript "*d*" indicates the divisor site. Here we assign station KSN, at which a large number of earthquakes were detected (Table 1), as the divisor site. We also made three assumptions in the inversion to obtain stable results; (A) station STG can be a reference rock site with no amplification [10] considering geological information and the shape of H/V spectral ratios of S-coda waves and microtremors, (B) event EQ053 (2015/07/09 18:32UTC; Mw5.6, depth=88 km) can be a reference event [12] whose seismic moment and corner frequency are known and the source spectrum can be modeled by omega-squared model [13] (here we used the values that were obtained from the moment tensor inversion by NIED), (C) KiK-net station FKS011 can be a reference site whose site amplification factor is known (http://www.ysk.nilim.go.jp/kakubu/kouwan/sisetu/site.html). By taking the logarithm on both sides of Eq. (2) and solving least square problems with the reference site constraint at each frequency, parameters $G_j(f)$ and $Q_S(f)$ are obtained.

3.3 Estimation of source, propagation path and site amplification factos

Figures 3 shows the estimated parameters $G_j(f)$ at 16 observation sites and two NIED stations. The estimated amplification factors $G_j(f)$ show spatial variations of site amplification in the area and the shapes correspond well to those of H/V spectral ratios of *S*- coda waves (20.48 s) for all stations. Station DJC and UMM are located to each other (260 m) but the characteristics of amplification factors (e.g. dominant frequencies and magnitudes) are significantly different to each other, indicating a drastic change of subsurface structure as stated in previous studies [4, 5]. On the other hand, the agreements between predominant frequencies of the estimated $G_j(f)$ and calculated ones from an existing structure model of seed sedimentary layers (J-SHIS model; http://www.j-shis.gosai.go.jp/) do not coincide at most of the stations, suggesting that the existing structure model is not sufficient to explain site amplification characteristics at individual site.

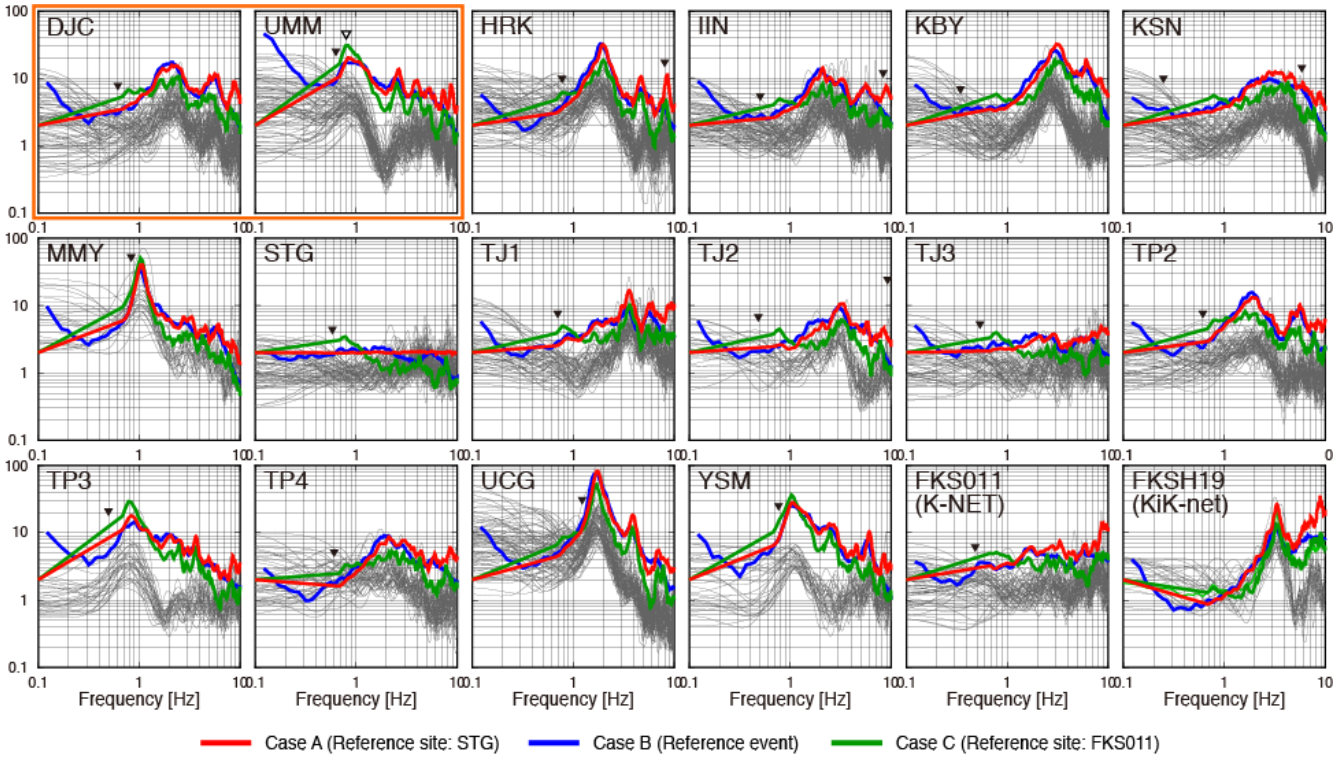

Fig. 3 – Estimated site amplification factors (red, blue and green traces) and calculated H/V spectral ratios of *S*-coda waves (gray traces). Black and white triangles indicate dominant frequencies calculated from J-SHIS structure model and our estimated model with microtremor array survey (only at station UMM), respectively.

To validate our inversion results, we also estimated source terms $S_i(f)$ from Eq. (1) using obtained $G_j(f)$ and $Q_S(f)$. We determined the flat levels of displacement source spectra Ω_0 from the estimated $S_i(f)$ and calculated seismic moment M_0

$$M_0 = \frac{4\pi\rho V_S^3}{R_{\theta\phi}}\Omega_0, \tag{3}$$

where $R_{\theta\phi} = 0.55$ is the radiation pattern, ρ and V_S are the density and the *S*-wave velocity around the hypocenter, respectively. We assigned the parameters ρ and V_S using the one-dimensional velocity structure model used for moment-tensor inversion by NIED [14]. Figure 4 shows a comparison between estimated seismic moment from automated moment tensor inversions (NIED CMT solutions) and those from the spectral inversion method with the assumption A. The comparison shows substantially good agreements between them. However, for large

earthquakes, our estimated seismic moment is slightly smaller than those estimated by NIED. This may suggest that the corner frequencies of the earthquakes are lower than the minimum frequency (0.3 Hz) in this study. Also, the estimated Q_S values indicate clear frequency dependent characteristics between 0.2 and 8 Hz, corresponding well to the proposed model in eastern Japan [15]. Here we obtained the relationship $Q_S(f)=68f^{1.12}$ from the regression line.

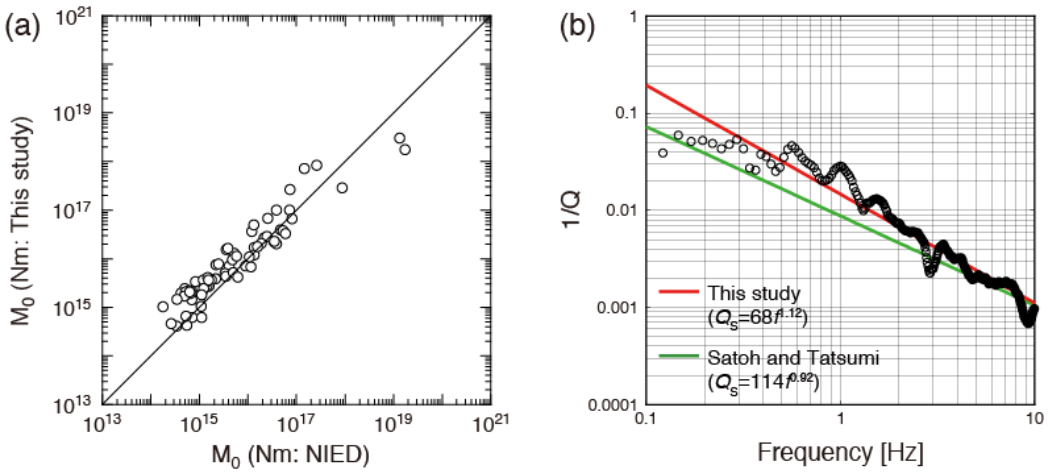

Fig. 4 – Comparisons of (a) estimated values of seismic moment and (b) Qs^{-1}.

4. Application of Seismic Interferometry to Microtremor Data

Recently the seismic interferometry technique using continuous long-term microtremor (ambient noise) records are widely applied to investigate the characteristics of surface wave propagation inside sedimentary basin and the accuracy of shear wave velocity structure model [e.g. 16-19]. Usually the technique is applied to microtremor data recorded at sufficiently isolated two stations in order to retrieve shorter wavelength characteristics compared to inter-station distances. In this study we apply the technique to data from the dense array to explore the possibility of the detection of surface-wave group velocity with much shorter wavelength (from several hundred meters to several kilometers). We used the continuous microtremor data recorded at stations HRK, KBY, KSN, MMY, STG, TP4 and UCG to investigate the accuracy of the existing subsurface velocity structure model beneath the city center. The station-to-station distances range from 2.0 km (KBY-KSN) to 9.3 km (KSN-UCG). First we divided the vertical components of the continuous waveforms into 655.36-second segments (=2^{16} data points) and applied one-bit normalization [20], after band-pass filtering at 0.2 to 2.0 Hz. We computed cross-correlation functions (CCFs) for seven station pairs where the same type of sensors are deployed.

Figure 5 shows examples of the stacked CCFs for six station pairs where SMAR-6A3P sensors are deployed and estimated Rayleigh-wave group velocities based on the multiple filtering technique (MFT) [21]. The stacked CCFs show clear and synmetric wave trains for the most station pairs. The estimated group velocities of Rayleigh wave show dispersive characteristics. For example, the velocities between station pairs HRK-UCG (west side) and HRK-KSN (east side) are largely different, suggesting the spatial variation of deep sedimentary structure model of the basin. For comparison, a theoretical dispersion curve of Rayleigh-wave group velocity is also calculated using one-dimensional velocity structure model of deep sedimentary layers (J-SHIS model; beneath station UMM). The estimated values are much smaller than the theoretical one, indicating subsurface *S*-wave velocity structure should be improved to explain the estimated characteristics properly.

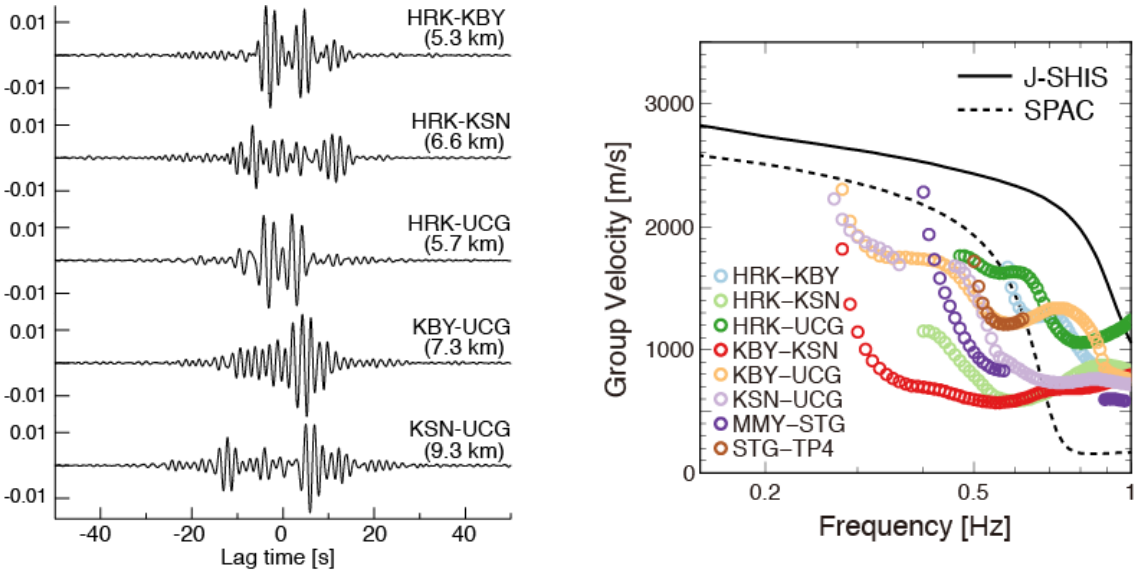

Fig. 5 – (left) Examples of the stacked cross-correlation functions (Z-Z component). (right) Estimated group velocities of Rayleigh waves for eight station pairs and theoretical dispersion curves calculated with J-SHIS (beneath station UMM) and our estimated model.

5. Discussion

5.1 Estimation of subsurface S-wave structure based on microtremor array survey

Our results from the spectral inversion method and seismic interferometry both suggest that the existing structure model (J-SHIS model) cannot explain dominant frequencies at most sites and group velocity dispersions of Rayleigh wave in the central part of the basin. This may indicate that the existing subsurface velocity structure is not modeled well and needed be improved. To investigate subsurface *S*-wave structure model and compare it with the existing ones, we conducted microtremor array survey in the central part of the basin. Here we applied the spatial autocorrelation (SPAC) method [22,23] to derive phase velocities of Rayleigh wave and estimated subsurface *S*-wave velocity structure. Two kinds of equilateral triangle arrays that consist of seven sensors with side lengths of 500 m and 1500 m (here we call these S-array and L-array, respectively) were deployed in January 24, 2016 (Fig. 6). The central points of the arrays are close to station UMM (city hall). We used feedback type seismometers VSE12-CC (500V/m/s: Tokyo Sokushin Ltd.) that cover down to 0.05 Hz with data logger McSEIS-MT (24bit A/D: OYO Corporation). Vertical component microtremors were observed with a sampling rate of 100 Hz, to estimate Rayleigh-wave phase velocities. The observations were continued one hour for S-array and two hours for L-array.

5.2 Comparison of estimated layered structure with existing ones

Figure 7a shows the estimated phase velocity of Rayleigh wave. We combined the estimated phase velocities from S- and L-arrays and results from previously obtained phase velocity dispersion curves with smaller array near station UMM [4] to obtain phase velocity dispersion curve in a wide frequency range. Based on the obtained phase velocity dispersion curve, we set a starting layered *S*-wave structure model consisting of 10 layers for the inversion, using the 1/3 wavelength rule of phase velocity. We applied a genetic algorithm [24] to find a best structure model that minimizes the misfit between determined and theoretical phase velocities of fundamental Rayleigh wave. Figure 7b shows the comparison between the final model with existing ones (extracted from the J-SHIS model) beneath the array. Our model indicates the existence of low *S*-wave velocity layers ($V_S \leq 350$ m/s) just beneath the ground surface (≤ 200 m), compared with the current models. Of course the J-SHIS structure is not constructed to include the low velocity layers, but the layers play important role to explain the phase velocity dispersion curve. We also calculated the dominant frequency and dispersion curve of

Rayleigh-wave group velocity using the estimated model. The calculated dominant frequency at station UMM coincides with the estimated one from the spectral inversion method (Fig. 3) and the theoretical dispersion curve of group velocity is substantially reasonable to explain the estimated ones from the seismic interferometry (Fig. 5). The comparisons indicate that the consideration of subsurface low-velocity layers is important to explain phase and group velocity properties as well as site amplification characteristics in Iwaki city.

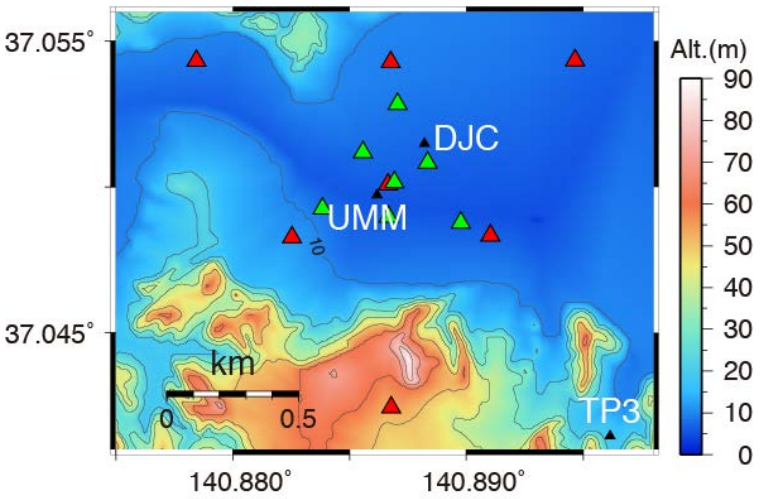

Fig. 6 – Locations of microtremor arrays (S-array: green triangles, L-array: red triangles).

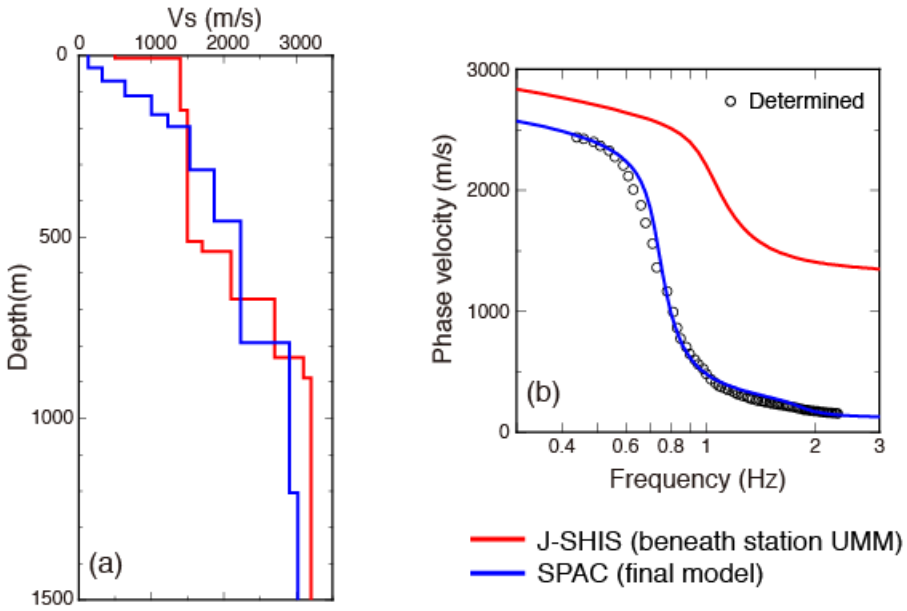

Fig. 7 – Comparisons of (a) velocity structures beneath station UMM and (b) corresponding phase velocity dispersion curves with determined phase velocity.

6. Conclusions

We deployed a dense seismic array in the central part of Iwaki city, Fukushima prefecture. The results from both the spectral inversion and seismic interferometry techniques indicate the spatial variations of subsurface soil structure in the area, suggesting that the consideration of subsurface layres with low velocity (several hundred

meters beneath the ground surface with $V_S \leq 350$ m/s) is important to explain the estimated characteristics of site amplifications and surface wave propagation characteristics. Our results indicate the necessity of structure model improvements in the area, based on further microtremor surveys (single and array observations), earthquake data analyses (e.g. spectral inversions with many stations, receiver function analysis [25]) or other possible geophysical surveys. The 1-year survey shows that the importance of model verification on a small scale and the combined use of the different approach with a dense array data provides beneficial information for model and improvements.

7. Acknowledgements

We used ground motion data from the K-NET and KiK-net as well as three-dimensional seismic velocity structure model provided by National Research Institute for Earth Science and Disaster Resilience (NIED), Japan. We also used the data of seismic intensities by Japan Meteorological Agency (JMA). The site amplification models at K-NET and KiK-net stations for verification are provided by Port and Harbor Department, National Institute for Land and Infrastructure Management, Ministry of Land, Infrastructure, Transport and Tourism, Japan. We used program package DISPER80 [26] for calculations of surface wave group velocities. Figures were plotted using Generic Mapping Tools [27].

7. References

[1] Kashima T, Koyama S, Okawa I (2012): Strong motion records in buildings from the 2011 off the Pacific coast of Tohoku earthquake. *Building Research Data*, **135**, Building Research Institute, Tsukuba, Japan (in Japanese with English abstract).

[2] Koketsu K, Miyake H, Fujiwara H, Hashimoto T (2008): Progress towards a Japan integrated velocity structure model and long-period ground motion hazard map. *Proceedings of the 14th World Conference on Earthquake Engineering*, Paper No.S10-038.

[3] Fujiwara H, Kawai S, Aoi S, Morikawa N, Senna S, Kudo N, Ooi M, Hao K, Hayakawa Y, Toyama N, Matsuyama H, Iwamoto K, Suzuki H, Liu Y (2009): A study on subsurface structure model for deep sedimentary layers of Japan for strong-motion evaluation. *Technical note of the National Research Institute for Earth Science and Disaster Prevention*, **337**, National Research Institute for Earth Science and Disaster Prevention, Tsukuba, Japan (in Japanese with English abstract).

[4] Wiradikarta CBM (2013): Underground velocity structure exploration using surface waves in Iwaki city hall, Japan. Master Thesis, National Graduate Institute for Policy Studies, Tokyo, Japan, pp. 37.

[5] Nakagawa H, Hayashida T, Yokoi T, Kashima T, Koyama S, Wiradikarta CBM, Guerra Carballo JR (2015): A microtremor exploration in Iwaki city hall for evaluation of inclined bedrock. *Journal of Japan Association for Earthquake Engineering*, **15** (7), 60-71 (in Japanese with English abstract).

[6] Japan Meteorological Agency (1996): On seismic intensity, Gyosei, pp.238 (in Japanese).

[7] Kinoshita S (1998): Kyoshin Net (K-NET). *Seismological Research Letters*, **69** (4), 309-332.

[8] Aoi S, Obara K, Hori S, Kasahara K, Okada Y (2000) : "New strong-motion observation network: KiK-net." *EOS. Transactions, American Geophysical Union*, **81**, F863.

[9] Okawa I, Satoh T, Sato T, Tohdo M, Kitamura H, Torii S, Tsuji Y, Kitamura Y (2013): Study on long-period ground motions and responses of super-high-rise buildings etc. -Proposal of updated empirical equations for long-period ground motions and evaluation of responses of super-high-rise and seismically isolated buildings under the hypothetical Nankai-Tonankai-Tokai connected earthquakes. *Building Research Data*, **144**, Building Research Institute, Tsukuba, Japan (in Japanese with English abstract).

[10] Iwata T, Irikura K (1988): Source parameters of the 1983 Japan Sea earthquake sequence. *Journal of Physics of the Earth*, **36** (4), 155-184.

[11] Husid RL (1969): Características de Terremotos, Análisis General. *Revista del IDIEM* **8**, Santiago, Chile, 21–42.

[12] Moya A, Irikura K (2003): Estimation of site effects and Q factor using a reference event. *Bulletin of the Seismological Society of America*, **93** (4), 1730–1745.

[13] Brune JN (1970): Tectonic stress and the spectra of seismic shear waves from earthquakes. *Journal of Geophysical Research*, **75** (26), doi: 10.1029/JB075i026p04997.

[14] Fukuyama E, Ishida M, Dreger DS, Kawai H (1998): Automated seismic moment tensor determination by using on-line broadband seismic waveforms, *Zisin (Journal of the Seismological Society of Japan. 2nd ser.)*, **51** (1), 149-156 (in Japanese with English abstract).

[15] Satoh T, Tatsumi Y (2002): source, path, and site effects for crustal and subduction earthquakes inferred from strong motion records in Japan. *Journal of Structural and Construction Engineering*, **556**, 15-24 (in Japanese with English abstract).

[16] Ma S, Prieto GA, Beroza GC (2008): Testing community velocity models for southern California using the ambient seismic field. *Bulletin of Seismological Society of America*, **98** (6), 2694–2714.

[17] Shapiro NM, Campillo M (2004): Emergence of broadband Rayleigh waves from correlations of the ambient seismic noise. *Geophysical Research Letters*, **31** (7), L07614, doi: 10.1029/2004GL019491.

[18] Yamanaka H, Chimoto K, Moroi T, Ikeura T, Koketsu K, Sakaue M, Nakai S, Sekiguchi T, Oda Y (2010): Estimation of surface-wave group velocity in the southern Kanto area using seismic interferometric processing of continuous microtremor data. *BUTSURI-TANSA (Exploration Geophysics)*, **63** (5), 409–425 (in Japanese with English abstract).

[19] Hayashida T, Yoshimi M, Horikawa H (2013): Estimation of surface wave group velocity beneath the Chukyo area, Japan - Application of seismic interferometry to Hi-net continuous waveform data-, *Zisin (Journal of the Seismological Society of Japan. 2nd ser.)*, **66** (4), 127-145 (in Japanese with English abstract).

[20] Sabra KG, Gerstoft P, Roux P, Kuperman WA, Fehler MC (2005): Extracting time-domain Green's function estimates from ambient seismic noise. *Geophysical Research Letters*, **32** (3), L03310, doi:10.1029/2004GL021862.

[21] Dziewonski A, Bloch S, Landisman M (1969): A technique for the analysis of transient seismic signals. *Bulletin of the Seismological Society of America*, **59** (1), 427–444.

[22] Aki K (1957): Space and time spectra of stationary stochastic waves, with special reference to microtremors. *Bulletin of the Earthquake Research Institute*, **35**, 415-456.

[23] Okada H (2003): The microtremor survey method, *Geophysical Monograph*, **12**, Society of Exploration Geophysicists, Tulsa.

[24] Yamanaka H, Ishida H (1996): Application of genetic algorithms to an inversion of surface-wave dispersion data. *Bulletin of the Seismological Society of America*, **86** (2), 436–444.

[25] Kobayashi K, Uetake T, Mashimo M, Kobayashi H (1998): An investigation on detection method of P to S converted waves for estimating deep underground structures. *Journal of Structural and Construction Engineering*, **505**, 45-52 (in Japanese with English abstract).

[26] Saito M (1988): DISPER80: A subroutine package for the calculation of seismic normal mode solutions. in Seismological Algorithms, edited by D. J. Doornbos, Academic Press, 293–319.

[27] Wessel P, Smith WHF, Scharroo R, Luis JF, Wobbe F (2013), Generic Mapping Tools: Improved version released, *EOS. Transactions, American Geophysical Union*, **94**, 409-410.